Energy Proceedings
Vol 58, 2025
ISSN 2004-2965

Investigation of overall cooling effectiveness on a steam-cooled double-wall vane of hydrogen gas turbine with mist injections#

Ran Bi[1], Jizhou Chen[1], Dehai Kong[1*], Shuo Ren[2], Sergey Isaev[3], Cunliang Liu[1*]

1 Northwestern Polytechnical University, Xi'an 710072, Shaanxi, China

2 Lomonosov Moscow State University, Moscow, 119991, Russia

3 Basic Research Laboratory, Saint-Petersburg State University of Civil Aviation, Saint-Petersburg, 196210, Russia

(Corresponding Author: kongdehai@nwpu.edu.cn, liucunliang@nwpu.edu.cn)

ABSTRACT

Numerical studies were conducted to investigate the conjugate heat transfer characteristics of a mist/steam-cooled high-pressure turbine vane in a hydrogen gas turbine, which was proposed for a hydrogen fuel pure oxygen combustion gas turbine combined cycle with flow bypass and recompression. A double-wall cooling vane operating in a real turbine environment was considered. The effect of mist injections on the overall cooling effectiveness of the steam-cooled double-wall vane of a hydrogen gas turbine was investigated by varying the mist concentration (5% ≤ m_s ≤ 20%) and droplet size (5 µm ≤ d_p ≤ 20 µm). The m_s and d_p have a synergistic effect on the overall cooling effectiveness, and it tends to increase with increasing m_s, especially at the suction side. The highest averaged overall cooling effectiveness of the steam-cooled vane at the mid-span of the vane was obtained at m_s = 20% with a relatively small particle size of 10 µm, which was approximately 11% higher than that without mist, corresponding to an 88.6K drop in the vane's wall temperature.

Keywords: hydrogen gas turbine, vane steam-cooling technology, conjugate heat transfer, mist injection

NOMENCLATURE

Abbreviations	
DRW	Discrete random walk
HPT	High-pressure turbine
LE	Leading edge
PS, SS	Pressure and suction side
Symbols	
d_p	Droplet size (µm)
m_s	Mist concentration
θ	Overall cooling effectiveness

1. INTRODUCTION

The transition to low-carbon energy systems has emerged as a critical development direction. To achieve the goal of carbon neutrality by 2060, a decarbonization plan for renewable-based electrical power systems has been proposed in China to reduce CO_2 emissions [1]. Recognized as a high-efficiency and clean energy source, hydrogen energy has garnered significant attention as a potential solution. The utilization of hydrogen-fueled gas

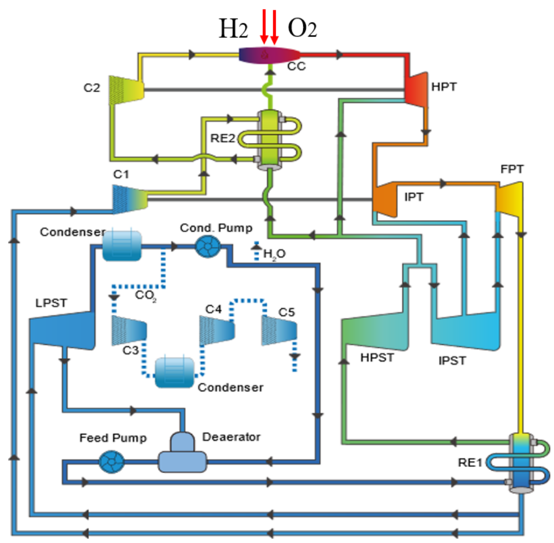

Fig. 1 Hydrogen fuel pure oxygen combustion gas turbine combined cycle [3]

turbine power generation offers a notable advantage due to its lower pollution and zero CO_2 emissions [2]. Fig. 1 illustrates a schematic view of an advanced gas turbine combined cycle configuration (R-Graz cycle) employing a high-efficiency shunting-recompression process and pure hydrogen fuel in pure oxygen combustion

This is a paper for the 11th Applied Energy Symposium: Low Carbon Cities & Urban Energy Systems (CUE2025), July 18-22, 2025, Kitakyushu, Japan.

technology. The detailed thermodynamic and economic analysis of this cycle has been reported by Yu et al. [3]. The use of pure hydrogen fuel and pure oxygen results in the combustion product being pure water vapor, eliminating CO_2 emissions.

Developing new efficient cooling technologies based on two-phase evaporative cooling [4, 5] and adopting a new cooling medium are two effective ways to improve the cooling capability of the turbine vane. Steam offers enhanced heat transfer performance with its substantially higher specific heat capacity than air [6]. The application of transported mist through the outer casing and disk cavity to cool turbine blades with droplet evaporation presents significant potential [7].

The objective of the present study was to explore the effect of the mist injections on the overall cooling effectiveness of the mist/steam-cooled double-wall HPT vane of a hydrogen gas turbine based on the R-Graz cycle.

2. NUMERICAL STUDY

2.1 Physical model

Fig. 2 shows the schematic view of the steam-cooled double-wall vane and its cooling configuration. The number of the HPT vane is 40, and the height and chord length (C) of the vane are 180 mm and 285 mm, respectively. The coolant secondary jet enters the first cavity from the vane's bottom side and the secondary cavity from the vane's top side entrance, respectively. At the first cavity, the coolant flows through the jet holes, impinging on the inner wall of the blade, and then is discharged out through the film holes on the blade surface, forming a film cooling near the external surface of the vane. At the secondary cavity, one part of the coolant, after flowing through the impinging jet holes, effused out through the film holes at the pressure side and suction side of the vane, and the other part of the coolant flowed out through the trailing edge cutback structure and is mixed with the main gas. Two rows of cylindrical dense film holes (LE1-LE2) and a row of laid-back dense film holes (LE3) towards PS with staggered configurations were arranged at the vane leading edge region, similar to the showerhead film cooling [8]. The flow angle of all the film holes is set to 45°. There are two rows of cylindrical film holes on the suction side of the vane (SS1-SS2) along the streamwise direction. Two rows of laid-back fan-shaped film holes are, respectively, arranged at the pressure side of the vane near the blade's leading edge (PS1 and PS2). All the film holes have a diameter of 2.7mm. At the trailing edge of the vane, the circular pin fin cooling structure combined with the jet orifice plate is used to enhance the internal heat transfer.

2.2 Boundary conditions

The high temperature and pressure in real gas turbine conditions [9] were imposed in the calculational model, as shown in Fig. 3. The mainstream is assumed to be the dry steam and has a uniform total pressure and

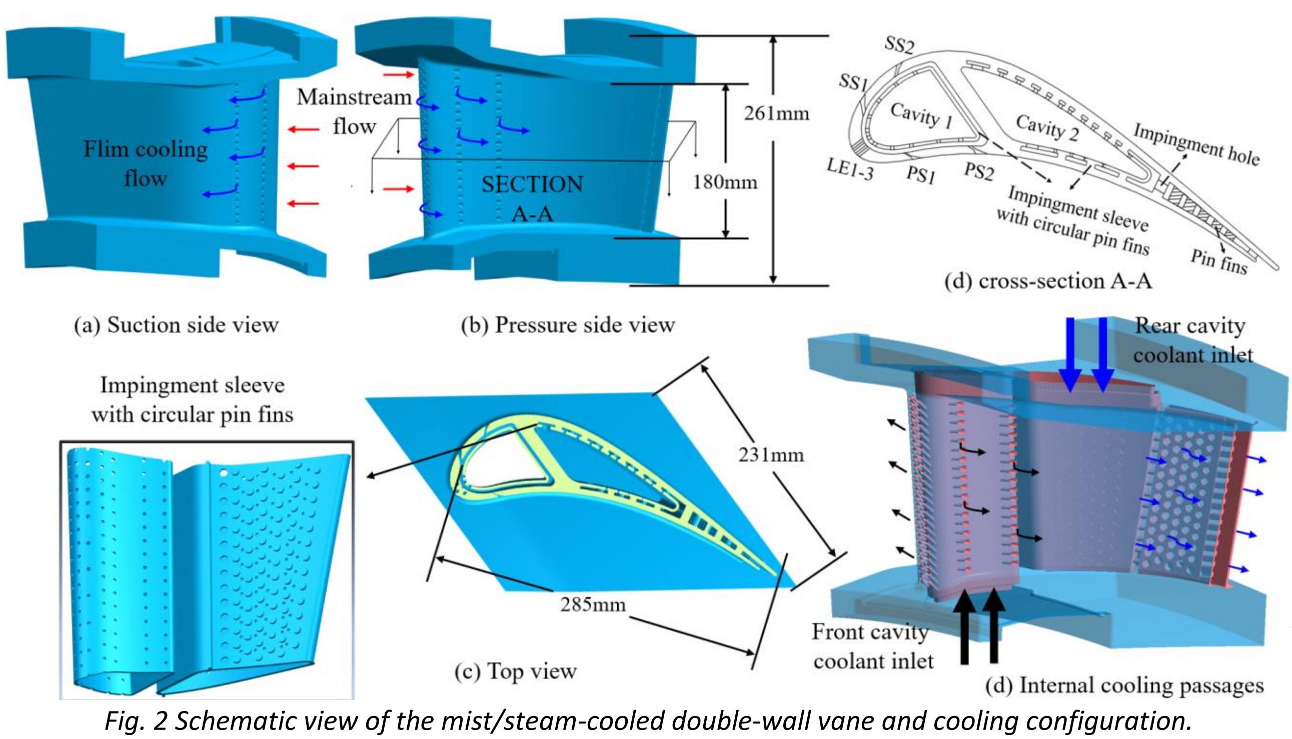

Fig. 2 Schematic view of the mist/steam-cooled double-wall vane and cooling configuration.

temperature of 3.8 MPa and 1773.2 K at the cascade passage inlet, respectively. The inlet turbulent intensity of the mainstream is set as 5%. The static pressure of 3.68 MPa was assigned at the cascade outlet. The cooling steam flow supplied by a coolant plenum is set as 0.38kg/s with a coolant-to-hot gas mass flow ratio of 4.8%, and one part at the front cavity inlet is 0.2 kg/s, the other part at the rear cavity inlet is 0.18 kg/s. The total temperature of the steam coolant at the two inlets is 567.52 K. The circumferential direction is assigned as the periodic boundary conditions, and all other walls are adiabatic and have a non-slip velocity boundary condition. As a conjugate boundary condition, the inner and outer surface of the turbine vane was established to satisfy the relationship between heat flux and temperature at the fluid-solid interface, and the endwalls are designated as adiabatic walls with non-slip conditions.

In addition, for the discrete droplet phase, the water mist concentration varies by 5%, 10%, and 20% at the coolant inlet. The mist droplet temperature is assigned as 300 K. The mass rate of the injection water droplet through the supply plenum was determined according to the product of the mist concentration and the mass rate of the coolant steam flow. Since the mist evaporation is strongly affected by the droplet size, the effect of uniform particle sizes of 5 μm, 10 μm, and 20 μm is considered. Furthermore, a reflecting boundary condition is set to simulate the interaction of the water droplet impingement with the wall [7, 10], and the coalescence effect of the droplet is also neglected to reduce the computational time.

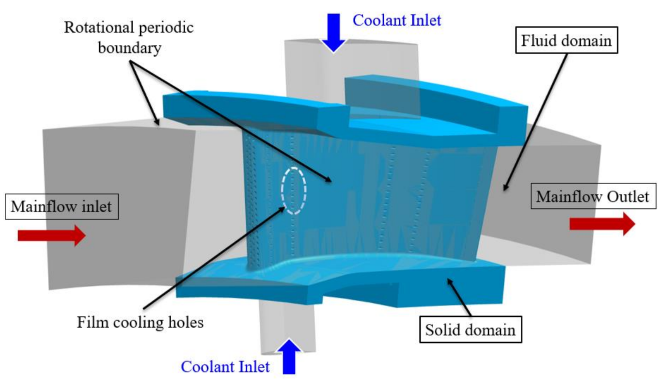

Fig. 3 Computational domain and boundary conditions for mist/steam-cooled vane.

2.3 Numerical methodology

The commercial software package ANSYS Fluent 18.0 was used to obtain the conjugate heat transfer characteristics of the vane with air and mist/steam turbulent flow. The solved region contains the solid vane and fluid domains of the mainstream and the secondary flow. For the fluid domain, turbulent flow and heat transfer were calculated based on the steady Reynolds-averaged Navier-Stokes (RANS) approach in combination with the SST γ-Re_ϑ four-parameter transition turbulence model due to its good prediction performance for turbulent flow and heat transfer in a cascade passage [8]. The radiation heat transfer of the air and steam flow in the cascade passage was ignored. In the case of mist injections, since the volume fraction of the liquid droplet particle was small, the Euler-Lagrangian discrete random walk (DRW) particle tracking multiphase simulation technique was applied [10].

The double-wall vane is modelled as a solid region and made of high-temperature superalloy GH625, whose thermophysical characteristics can be referenced in [11]. In addition, during the simulation, the density of air and steam was determined by solving the ideal gas equation. The dynamic viscosity and thermal conductivity of the air and steam were obtained from the NIST Real Gas model, expressed as functions of temperature. Conversely, the thermophysical properties of the discrete phase (liquid droplets) were determined using the IAWPS-IF97 formulation [12].

2.4 Mesh generation

The unstructured tetrahedral grids were created for the computational domain with an air-cooled turbine vane due to the complex internal cooling passage in it. The grids of the vane solid region and fluid region were generated separately and then integrated through interface connections to achieve the coupling analysis. A finer grid was used in the boundary layer region near the surface of the turbine vane, ribs, pin-fins, film holes, and impingement holes. The height of the first layer of mesh is set as 0.01mm, and the growth rate is 1.15, to ensure that the y+ value of the first layer of the grid is smaller than 1, which meets the SST γ-Reθ model's requirement of mesh in the boundary layer. After the mesh independence check study, the element number of about 4.8 M was selected for further study.

2.5 Data reduction

The overall cooling effectiveness (ϑ) is calculated by

$$\theta = \left(T_g - T_w\right) / \left(T_g - T_c\right) \tag{1}$$

where T_g is the temperature of the hot gas, and T_c is the coolant temperature at the plenum cavity inlet, T_w is the external wall temperature of the vane.

3. RESULTS

3.1 Influence of mist concentrations

Fig. 4 shows the distribution of the cooling effectiveness at the vane mid-span at different mist concentrations with d_p =10 μm. It can be seen that, generally, the case with a higher mist ratio of 20% provides the highest cooling effectiveness at most regions of the vane. At SS, with the mist concentration increases, the cooling effectiveness tends to gradually increase due to the droplets' evaporation increasing the mass flow rate of the coolant steam and reducing the coolant temperature, as well as reducing the heat load transferred from the hot mainstream to the vane wall as a result of the latent heat absorption. However, at the vane PS and leading edge region, the effect of the mist proportion differs significantly. In the vane leading edge region at PS (-0.2 < X/C < 0), with increasing the mist ratio to 5%, the cooling effectiveness increases, and further increasing the mist ratio to 10%, it sharply decreases and then tends to be stable as the mist ratio increases to 20%. The highest cooling effectiveness was obtained for the case with 5% mist injection mainly because at a relatively high mist concentration ($m_s \geq 10\%$), a large number of droplets may block the film holes and prevent the cooling film from flowing out through the film holes, leading to a reduction of the film cooling effect and overall cooling effectiveness at the corresponding region.

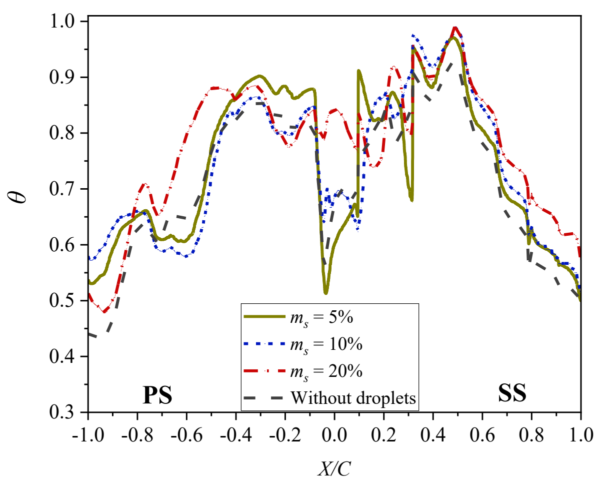

Fig. 4 Comparison of cooling effectiveness along the mid-span of the vane for different m_s

3.2 Influence of droplet size

Fig. 5 shows the effect of the mist concentration and particle size on the distributions of the cooling effectiveness at the vane mid-span. At SS, near the trailing edge of the vane (0.5 < X/C < 1.0), the cooling effectiveness increases with the droplet size. This is because the droplets with larger sizes travel a longer distance as they flow out from the film holes, which leads to a larger film coverage area downstream of the film holes. At the vane leading edge region (-0.3 < X/C < 0.3), the optimal particle size for the highest cooling effectiveness at the vane mid-span was 10 μm. Meanwhile, the excessive water droplets may block the film holes at the leading region, weakening the film coverage effect of the cooling steam. At PS, near the trailing edge (-1.0 < X/C < -0.8), the optimal particle size was obtained for the small droplet at d_p = 10 μm.

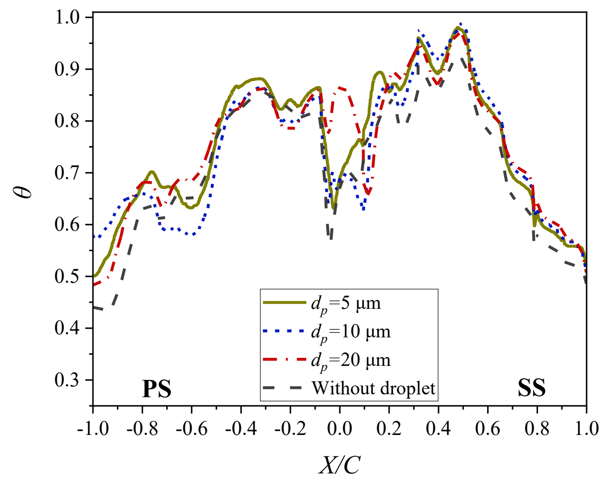

Fig. 5 Comparison of cooling effectiveness along the mid-span of the vane for different d_p

3.3 Droplet dynamics

Fig. 6 illustrates the distributions of the cooling effectiveness and streamlines with mist on the surface (a) and inside (b) of the vane. From Fig. 5a, it can be seen that most of the water droplets evaporate in the internal chamber of the vane, and a small number of droplets flow out from the film holes. The exception is at SS, where more water droplets bleed out from the film holes of SS1 and SS2 due to the relatively smaller pressure as compared to that at PS. Consequently, the improvement of the cooling effectiveness on the SS is higher than that on other regions of the vane due to the mist injection. Fig. 5b shows that the water droplets mainly interact with the impingement chamber of the double-wall cooling at the leading edge and mid-chord regions, leading to significant internal heat transfer enhancement at the corresponding regions.

3.4 Overall cooling effectiveness

As depicted in Fig. 7, the spanwise averaged cooling effectiveness along the mid-span gradually increases with the mist proportions under all the investigated droplet sizes in both cases. The maximum spanwise averaged cooling effectiveness of 0.759 at the mid-span was obtained at the mist ratio of 20% with a particle size of 10 μm, which is approximately 10.8% higher than that

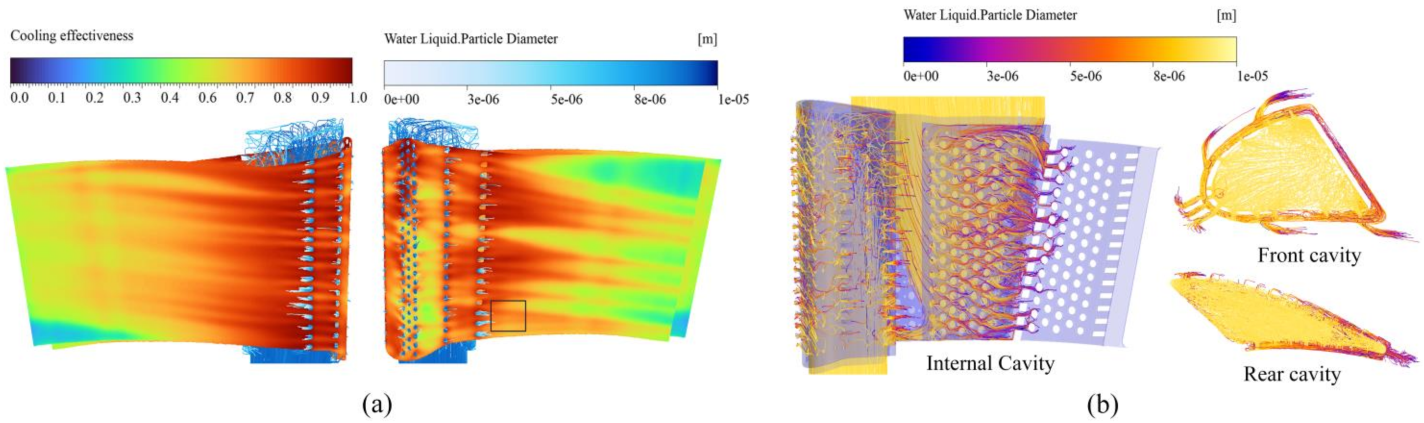

Fig. 6 Distributions of the cooling effectiveness and streamlines with mist on the surface (a) and inside (b) of the vane.

of the case without mist, and correspondingly, the average temperature at the mid-span dropped by 88.6 K. The worst improvement of the cooling effectiveness was observed at a 5% mist ratio with a particle size of 20 µm, which is only 3.4% higher than that of the case without mist, with a 28.1K temperature drop of the average temperature at the mid-span. The effect of the particle size on the average overall cooling effectiveness at the mid-span is not significant. At relatively low mist ratios ($m_s \leqslant 10\%$), the cooling effectiveness tends to slightly increase with the increase of the particle diameter. However, at high mist ratios (ms =10%), with the increase of the particle size, the cooling effectiveness firstly slightly increases, and then sharply decreases as particle size rises to dp = 20 µm. This is mainly due to the high mist ratio with large particles that may block the film holes, and the droplets are difficult to completely evaporate and fly off the vane surface, leading to a small contribution to improving the film coverage. These, in verse, reduce the cooling effectiveness of the vane.

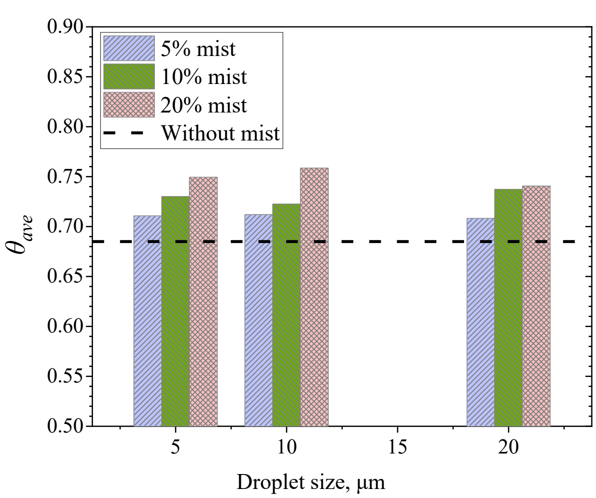

Fig. 7 Variations of the averaged cooling effectiveness along the mid-span of the vane

4. CONCLUSIONS

In the present study, the overall cooling effectiveness on the surface of the mist/steam-cooled double-wall vane of a hydrogen gas turbine was numerically examined at three different mist concentrations (5%, 10%, and 20%) and droplet sizes (5 µm, 10 µm, and 20 µm). The following conclusions can be drawn from the present study:

(1) The effect of mist concentration varies across the different regions of the vane, while generally showing an increasing trend as the mist concentration increases, especially at SS due to the relatively low pressure. The highest averaged overall cooling effectiveness at the mid-span was obtained at the mist concentration of 20% with a particle size of 10 µm, showing about 11% higher than that of the case without mist; correspondingly, a maximum of average temperature drop of 88.6 K at the mid-span was observed.

(2) The particle size has little effect on the average cooling effectiveness of the vane at the mist ratio changing from 5% to 20%. For small particles ($d_p \leq 5$ µm), the water droplet may completely evaporate at the impingement sleeve, and only a small number of them were discharged from the film holes, which slightly improves the film coverage effect. For the large particles ($d_p \geq 20$ µm), the relatively longer droplet's lifetime causes the droplets that be hard to improve the film cooling coverage effect on the vane surface due to the droplet evaporation since the strong particle inertia easily leads them to fly away from the vane surface. Therefore, to make the mist at full capacity to improve the overall cooling effectiveness of the vane, a proper particle size should be adopted.

Notably, the addition of mist enhances film cooling performance on the vane surface, resulting in higher overall cooling effectiveness and reduced coolant consumption. A high mist concentration coupled with a nonuniform droplet size distribution is considered effective in preventing coolant detachment from the wall, promoting improved film coverage and cooling uniformity in the extended downstream region of the film holes on both the pressure and suction sides of the vane. However, excessive mist concentration may negatively impact vane longevity due to increased corrosion potential from mist deposition on the surface. Further multi-physics coupling analysis is required to draw definitive conclusions regarding this aspect.

ACKNOWLEDGEMENT

This work received support from the National Natural Science Foundation of China (Grants nos. 52476092, U2241268, and U2241251).

REFERENCE

[1] Luo S, Hu W, Liu W, Zhang Z, Bai C, Huang Q, Chen Z, Study on the decarbonization in China's power sector under the background of carbon neutrality by 2060. Renew Sust Energ Rev 2022; 166: 112618.

[2] Zhou H, Xue J, Gao H, Ma N. Hydrogen-fueled gas turbines in future energy system, Int J Hydrogen Energ 2024; 64: 569–582.

[3] Yu S, Ren X, Hu B, Gu C. Investigation of control strategies for the hydrogen fueled R-Graz cycle, Int J Hydrogen Energ 2024; 92: 260–269.

[4] Biswal P, Mallikarjuna P, Balaji C. Research advances on mist assisted impingement and film cooling of turbine blades, Int J Heat Mass Transf 2024; 232: 125907.

[5] Varaksin AY. Hydrogasdynamics and thermal physics of two-phase flows with solid particles, droplets, and bubbles, High Temp 2023; 61: 852-870.

[6] Zeng J, Ma C, Lai C, Gao T, Gong J, Zhai G. Investigation on the flow and heat transfer of mist/steam cooling in two-pass ribbed channels with various aspect ratios, Int Commun Heat Mass Transfer 2024; 156: 107693.

[7] Zhao L, Wang T. An experimental study of mist/ air film cooling on a flat plate with application to gas turbine airfoils-part I: Heat transfer. J Turbomach 2014; 136: 071006.

[8] Xu Z, Liu C, Ye L, Zhu H, Wu Z. Investigation of the effect of combustor swirl flow on turbine vane full coverage film cooling. Energy 2024; 295: 130965.

[9] Qiao C, Li G, Zhang W, He H, Duan F, Wang P. Experimental study on the overall cooling effectiveness of nozzle guide vane under high temperature and high pressure. Case Stud Therm Eng 2022;33:101923.

[10] Abdelmaksoud R, Wang T. Simulation of air/mist cooling in a conjugate, 3-D gas turbine vane with internal passage and external film cooling. Int J Heat Mass Transf 2020; 160: 120197.

[11] Donachie MJ, Donachie SJ. Superalloys: a technical guide, 2nd ed. Ohio: ASM International; 2002, p. 11–24.

[12] Harvey A, Parry WT, Bellows JC, Gallagher JS, Harwood RD. ASME international steam tables for industrial use. 3rd ed. ASME Press, New York: NY; 2014.